Emergent constraint on the projected central tropical Pacific warming and northwestern Pacific monsoon trough change

Tao Tang (jscztangtao@hotmail.com)
Institute for Climate and Application Research (ICAR), Nanjing University of Information Science and Technology
Li Qi
Key Laboratory of Meteorological Disaster of Ministry of Education/Joint International Research Laboratory of Climate and Environment Change/ Collaborative Innovation Center on Forecast and Evaluati
Tomoki Tozuka
The University of Tokyo https://orcid.org/0000-0001-6738-1299
Jing-Jia Luo
Nanjing University of Information Science and Technology https://orcid.org/0000-0003-2181-0638
Jinhai He
Nanjing University of Information Science and Technology

Article

Keywords: northwestern Pacific monsoon trough, tropical Pacific mean-state change, thermocline sharpness, CMIP6, emergent constraint method

Posted Date: August 2nd, 2023

DOI: https://doi.org/10.21203/rs.3.rs-3222878/v1

Additional Declarations: There is **NO** Competing Interest.

Emergent constraint on the projected central tropical Pacific warming and northwestern Pacific monsoon trough change

Tao Tang[1,2*], Li Qi[3], Tomoki Tozuka[4], Jing-Jia Luo[1,3], and Jin-Hai He[1,3]

[1] Institute for Climate and Application Research (ICAR), Nanjing University of Information Science and Technology, Nanjing 210044, China
[2] Zhejiang Meteorological Observatory, Hangzhou 310002, China
[3] Key Laboratory of Meteorological Disaster of Ministry of Education/Joint International Research Laboratory of Climate and Environment Change/Collaborative Innovation Center on Forecast and Evaluation of Meteorological Disasters, Nanjing University of Information Science and Technology, Nanjing 210044, China.
[4] Department of Earth and Planetary Science, Graduate School of Science, The University of Tokyo, Tokyo 113-0033, Japan.

*Corresponding author. E-mail: jscztangtao@hotmail.com

Abstract

The northwestern Pacific monsoon trough (NWPMT) deeply impacts socio-economic development and human security over East Asia by supplying moisture to the summer monsoon rainfall and modulating tropical cyclone activities. However, considerable inter-model spreads in the Coupled Model Inter-comparison Project Phase 6 models make the future projection of the NWPMT less reliable. Here, we find that the inter-model spread of the NWPMT change is significantly correlated with the central equatorial Pacific sea surface temperature change, and mainly determined by the equatorial thermocline sharpness in the historical simulations. According to the emergent constraint method, the central equatorial Pacific SST would warm up about 8% slower than the multi-model mean with 56% uncertainty reduced. Correspondingly, the NWPMT would slacken westward with 36% uncertainty reduced. Results here emphasize the importance of examining and reducing systematic model biases in simulating subsurface fields that have been overlooked in past literatures, before achieving more reliable future projections.

Keywords

northwestern Pacific monsoon trough, tropical Pacific mean-state change, thermocline sharpness, CMIP6, emergent constraint method.

Introduction

The northwestern Pacific monsoon trough (NWPMT) is associated with convergence of the southwesterly monsoon winds and the prevailing northeasterly trade winds over the northwestern tropical Pacific[1-4] in boreal summer. The induced weak vertical wind shear and cyclonic vorticity provide a favorable environment for the genesis and development of tropical cyclones (TCs) in boreal summer[5,6]. Therefore, anomalous shifts in the NWPMT location have great socio-economic impacts on East and Southeast Asia where billions of people live in[7-10].

Although state-of-the-art climate models cannot simulate key features of TCs to investigate the future change of TCs activities directly[11-13], it has been suggested that projected extension (withdrawal) of the NWPMT is a good indicator of more (less) strong TCs over the northwestern Pacific in boreal summer under global warming[10]. However, the projected zonal shifts of the NWPMT under global warming remain inconclusive due to considerable inter-model spreads in the projected tropical Pacific sea surface temperature (SST) change in the future[10].

The reliability of the tropical Pacific SST change in the latest climate models suffers from systematic biases[14-23]. While previous works focused on biases in simulating the climatological SST[19,20,22-25], air-sea feedbacks[19,21,22], and interactions among tropical oceans[18,19], biases in simulating the subsurface ocean of the tropical Pacific have not been examined yet. With respect to the tropical Pacific SST change, the slow response to the anthropogenic forcing in the subsurface may be more important than the fast response in the atmosphere[26-29], and the biases in the subsurface may thus have more important and straightforward impacts.

Here, we suggest for the first time that the inter-model spreads in the projected central equatorial Pacific SST and NWPMT changes are significantly correlated with the simulated equatorial Pacific thermocline sharpness in the Coupled Model Inter-comparison Project Phase 6 (CMIP6) models. Based on the emergent constraint method[20-23,32,33,38], we show that the central tropical Pacific SST is projected to warm up about 8% slower than the raw projection with about 56% reduction in uncertainty. Correspondingly, the NWPMT is projected to slacken westward under global warming with about 36% reduction in uncertainty.

Results

The cross-equatorial flows turn into the southwesterly wind over the South China Sea (SCS), and converge with the prevailing easterly winds over the northwestern tropical Pacific in boreal summer (July-October). The induced positive relative vorticity extends southeastward from the SCS to the equatorial Pacific with negative relative vorticity lying on both sides (Fig. 1A). Following previous works[8,10], the NWPMT index is defined as the eastern-most longitude of zero-zonal wind contour within positive vorticity region at 850 hPa (Fig. 1A). The spatial pattern of the NWPMT in the CMIP6 multi-model mean (MME) in both the historical simulation[30] (Fig. 1B) and the Shared Socioeconomic Pathway (SSP) 245 scenario[31] (Fig. 1C) are similar to that in the observation.

The change of NWPMT index between SSP245 (2059-2098) and historical simulation (1981-2020) is used to represent the zonal shift of NWPMT (see "Methods"). Although the CMIP6 MME suggests that the NWPMT will extend slightly eastward in future, the inter-model spread is quite large. More specifically, half of 22 CMIP6 models project that the NWPMT would retreat westward, while other models project that it would extend further eastward (Fig. 1D).

Based on the high-quality observational datasets over the past 40 years, the zonal shift of the NWPMT seems to be not determined by the local SST anomaly, because the negative correlations between precipitation and SST anomaly signify that the SST anomaly is the response, rather than the forcing of the convective anomaly over the northwestern Pacific in boreal summer[34] (Fig. S1A). In fact, the interannual and interdecadal shifts of NWPMT are mainly determined by variabilities of the central equatorial Pacific SST (Figs. S1B, C). Consistently, the projected shift of the NWPMT is also significantly correlated with the projected change in the central equatorial Pacific SST (Fig. 2A).

Interestingly, the spatial pattern of the inter-model correlation coefficients between the projected shift of the NWPMT and the change in the equatorial Pacific SST can be well captured by the leading empirical orthogonal function (EOF) mode of the inter-model spread of the equatorial Pacific SST change; the pattern correlation coefficient reaches 0.92 (Figs. 2A, B). The leading EOF mode accounts for about 45% of inter-model variance among CMIP6 models, and shows the SST warming center over the central equatorial Pacific (Fig. 2B). Moreover, the projected shift of the NWPMT is significantly correlated with the principal component of the leading mode (PC1, Fig. 2C). According to the Matsuno-Gill response[35], the CMIP6 models that project a faster SST warming over the central equatorial Pacific, by strengthening the westerly winds, positive relative vorticity, and rainfall over the northwestern tropical Pacific (Fig. S2), would thus project a larger eastward shift of the NWPMT (Fig. 2C).

To unravel the root cause of the inter-model uncertainty in central equatorial Pacific SST change, correlation coefficients between the PC1 and the vertical potential ocean temperature gradient (i.e.,$\frac{dT}{dz}$) in the historical simulations are examined. It is found that both meridionally and zonally averaged correlation coefficients are significantly negative along the thermocline (Figs. 3A, B). More specifically, the CMIP6 models with larger vertical ocean temperature gradient across the thermocline in the historical simulation correspond to a smaller PC1, and would project a slower central equatorial Pacific SST warming in the future. Hereafter, the vertical temperature gradient across the thermocline in each model is measured by the depth between 20°C and 16°C isotherms, and called the thermocline sharpness.

According to the emergent constraint method[32,33,38] (see "Methods"), the thermocline sharpness in the observed datasets can be used to derive a more robust and reliable central equatorial Pacific SST change than that in the original projection in the CMIP6 MME (Fig. 4A). It is found that only 4 out of 22 CMIP6 models locate within the range of three observed and assimilated datasets and could thus realistically simulate the thermocline sharpness, while 4 models simulate excessively sharp thermocline and 14 models simulate too diffuse thermocline. The PC1 constrained by the observed thermocline sharpness equals about -1.75, while the raw one projected by the CMIP6 MME equals to 0. Accordingly, the projected central equatorial Pacific SST change in boreal summer after emergent constraint would warm slower than that projected by the MME (Fig. S3A).

The physical mechanism underpinning the emergent constraint method may be explained as follows: The CMIP6 models with sharper thermocline have larger vertical temperature gradient across the thermocline, and thus could cool the SST more efficiently by the thermocline feedback[36] (Fig. 3). Compared with the CMIP6 models with more diffuse thermocline, the SST warming due to the anthropogenic forcing over the central-eastern equatorial Pacific would be greatly damped in the CMIP6 models with realistic thermocline sharpness. The induced faster SST warming over the western equatorial Pacific than that over the central-eastern equatorial Pacific would further benefit the slower SST warming over the central-eastern equatorial Pacific according to the Bjerknes feedback[37] (Fig. 4A).

In addition, the uncertainty in PC1 of equatorial Pacific SST change can also be greatly reduced after emergent constraint[32,38]. The probability density function of standardized PC1 can be assumed to have a Gaussian distribution with a mean of zero and a standard deviation of 1 (Fig. 5A). Since the inter-model correlation coefficient between the projected PC1 and the simulated thermocline sharpness reaches 0.75 (Fig. 4A), the variance explained by the PC1 is about 56% of the total variance. The residual variance of the PC1 is 44% of the total variance, and the standardized PC1 after emergent constraint still has a Gaussian distribution but with a mean of -0.35 and a standard deviation of 0.66 (Fig. 5A). Thus, the equatorial Pacific SST is projected to warm up about 8% slower than the MME, and its uncertainty is reduced by 56% after constraining the thermocline sharpness along the equatorial Pacific.

The more diffuse thermocline simulated in the CMIP6 MME would also exaggerate the projected expansion of the NWPMT under global warming (Fig. 4B). More specifically, the CMIP6 models with more diffuse thermocline would project faster SST warming over the central equatorial Pacific, and further result in stronger westerly winds and thus stronger positive vorticity over the NWPMT region. Correspondingly, the NWPMT would expand more to the east under global warming. On the other hand, the projected NWPMT in all of the 4 models with realistic thermocline sharpness will slacken westward in the future (Fig. 5B). As a result, the NWPMT after emergent constraint would retreat westward in the future, in contrast with the slight eastward expansion of the NWPMT projected by the CMIP6 MME (Fig. S3B). Moreover, the uncertainty in the projected shift of the NWPMT is reduced by 36%, because the inter-model correlation coefficient between the NWPMT change and thermocline sharpness is 0.60 (Fig. 5B).

Summary and discussion

Changes in the zonal location of the NWPMT have great socio-economic impacts on East Asia. However, without a reliable future projection of the NWPMT change, no proper measures for disaster prevention and mitigation can be undertaken. Our results here suggest that the SST over the central equatorial Pacific would warm up slower than the CMIP6 MME projection with about 56% uncertainty reduced, and the NWPMT would slacken westward with about 36% uncertainty reduced by constraining thermocline sharpness along the equatorial Pacific. Considering the anti-phase shift of NWPMT and northwestern Pacific Subtropical high (NWPSH), our results here are in agreement with the previous work that projected the future strengthening of the NWPSH[32].

Although the mechanism underpinning the emergent constraint method is straightforward and easy to understand, the cause of the systematic bias in simulating the thermocline sharpness[39,40] requires further investigations.

References

1. Wang, B., Chan, J.C.L. & Xu, X. Northern Hemisphere summer monsoon singularities and climatological intra-seasonal oscillation. *J. Clim.* **10,** 1071-1085 (1997).
2. Wu, R. & Wang, B. Multi-stage onset of the summer monsoon over the western North Pacific. *Clim. Dyn.* **17,** 277-289 (2001).
3. Feng, T. et al. Reexamination of the climatology and variability of the Northwest Pacific monsoon trough using a daily index. *J. Clim.* **33,** 5919-5938 (2020).
4. Qin, C. et al. A mechanism for formation of the western North Pacific monsoon trough: nonlinear upscale cascade. *Clim. Dyn.* **56,** 3889-3898 (2021).
5. Gray, W. M. Global view of the origin of tropical disturbances and storms. *Mon. Weather Rev.* **96,** 669-700 (1968).
6. Li, T. Synoptic and climatic aspects of tropical cyclogenesis in western North Pacific. Cyclones: Formation, Triggers and Control, *Oouchi, K., and H. Fudeyasu, Eds., Nova Science Publishers, Inc.* Hauppauge, NY, 61-94 (2012).
7. Wu, L. et al. Possible linkage between the monsoon trough variability and the tropical cyclone activity over the western North Pacific. *Mon. Weather Rev*. **140,** 140-150 (2012).
8. Qi, L. Decadal shift of the interannual relationship between western North Pacific tropical cyclone genesis frequency and South China Sea monsoon trough around 1980s. *Int. J. Climatol*. **42,** 4289-4299 (2021).
9. Liu, C. et al. Pacific meridional mode-western North Pacific tropical cyclone linkage explained by tropical Pacific quasi-decadal variability. *Geophys. Res. Lett.* **46,** 13346-13354 (2019).
10. Wang, C. & Wu, L. Future change of the monsoon trough: Sensitivity to sea surface temperature gradient and implications for tropical cyclone activities. *Earths Future* **6,** 919-936 (2018).
11. Camargo, S. J. Global and regional aspects of tropical cyclone activity in the CMIP5 models. *J. Clim.* **26**, 9880-9902 (2013).
12. Kossin, J. P., Emanuel, K. A. & Vecchi, G. A. The poleward migration of the location of tropical cyclone maximum intensity. *Nature* **509**, 349-352 (2014).
13. Walsh, K. J. E. et al. Hurricanes and climate: The U.S. CLIVAR working group on hurricanes. *Bull. Am. Meteorol. Soc.* **96**, 997-1017 (2015).
14. Luo, J.-J., Wang, G. & Dommenget, D. May common model biases reduce CMIP5's ability to simulate the recent Pacific La Niña-like cooling? *Clim. Dyn.* **50,** 1335-1351 (2018).
15. McGregor, S. et al. Model tropical Atlantic biases underpin diminished Pacific decadal variability. *Nat. Clim. Change* **8,** 493-499 (2018).
16. Kajtar, J. B. et al. Model under-representation of decadal Pacific trade wind trends and its link to tropical Atlantic bias. *Clim. Dyn.* **50,** 1-14 (2018).
17. Seager, R. et al. Strengthening tropical Pacific zonal sea surface temperature gradient consistent with rising greenhouse gases. *Nat. Clim. Change* **9,** 517-522 (2019).
18. Cai, W. et al. Pantropical climate interactions. *Science* **363,** eaav4236 (2019).
19. Tang, T. et al. Over-projected Pacific warming and extreme El Niño frequency due to CMIP5 common biases. *Natl. Sci. Rev.* **8,** nwab056 (2021).
20. Huang, P. & Ying, J. A multimodel ensemble pattern regression method to correct the tropical Pacific SST change patterns under global warming. *J. Clim.* **28,** 4706-4723 (2015).
21. Ying, J. & Huang, P. Cloud-radiation feedback as a leading source of uncertainty in the tropical Pacific SST warming pattern in CMIP5 models. *J. Clim.* **29,** 3867-3879 (2016).

22. Li, G. et al. Effects of excessive equatorial cold tongue bias on the projections of tropical Pacific climate change. Part I: the warming pattern in CMIP5 multi-model ensemble. *Clim. Dyn.* **47,** 3817-3831 (2016).
23. Park, I.-H. et al. Emergent constraints on future expansion of the Indo-Pacific warm pool. *Geophys. Res. Lett.* **49,** e2021GL097343 (2022).
24. Wang, C. et al. A global perspective on CMIP5 climate model biases. *Nat. Clim. Change* **4,** 201-205 (2014).
25. Samanta, D., Karnauskas, K. B. & Goodkin, N. F. Tropical Pacific SST and ITCZ biases in climate models: Double trouble for future rainfall projections? *Geophys. Res. Lett.* **46,** 2242-2252 (2019).
26. Xie, S.-P. et al. Global warming pattern formation: Sea surface temperature and rainfall. *J. Clim.* **23,** 966-986 (2010).
27. Luo, Y. et al. Understanding the El Niño-like oceanic response in the tropical Pacific to global warming. *Clim. Dyn.* **45,** 1945-1964 (2015).
28. Luo, Y. et al. The role of ocean dynamical thermostat in delaying the El Niño like response over the equatorial Pacific to climate warming. *J. Clim.* **30,** 2811-2827 (2017).
29. Ying, J., Huang, P. & Huang, R. Evaluating the formation mechanisms of the equatorial Pacific SST warming pattern in CMIP5 models. *Adv. Atmos. Sci.* **33,** 433-441 (2016).
30. Eyring, V. et al. Overview of the Coupled Model Inter-comparison Project Phase 6 (CMIP6) experimental design and organization. *Geosci. Model Dev.* **9,** 1937-1958 (2016).
31. O'Neill, B. C. et al. The scenario model intercomparison project (ScenarioMIP) for CMIP6. *Geosci. Model Dev.* **9,** 3461-3482 (2016).
32. Chen, X. et al. Emergent constraints on future projections of the western North Pacific subtropical high. *Nat. Commun.* **11,** 2802 (2020).
33. Li, G. et al. Western Pacific emergent constraint lowers projected increase in Indian summer monsoon rainfall. *Nat. Clim. Change* **7,** 708-712 (2017).
34. Wu, R.-G., Kirtman. B. & Pegion, K. Local air sea relationship in observations and model simulations. *J. Clim.* **19,** 4914-4932 (2006).
35. Gill A. Some simple solutions for heat-induced tropical circulation, *Q. J. R. Meteor. Soc.* **106,** 447-462 (1980).
36. Clement, A. C. et al. An ocean dynamical thermostat. *J. Clim.* **9,** 2190-2196 (1996).
37. Bjerknes J. Atmospheric teleconnections from the equatorial Pacific. *Mon. Weather Rev.* **97,** 163-172 (1969).
38. Bowman, K. W. et al. A hierarchical statistical framework for emergent constraints: application to snow-albedo feedback. *Geophys. Res. Lett.* **45,** 13050-13059 (2018).
39. Stockdale, T. N. et al. Ocean modeling for ENSO. *J. Geophys. Res.* **103**, 14325-14355 (1998).
40. Tatebe, H., & Hasumi, H. Formation mechanism of the Pacific equatorial thermocline revealed by a general circulation model with a high accuracy tracer advection scheme. *Ocean Model* **35**, 245-252 (2010).
41. Hersbach, H. et al. The ERA5 global reanalysis. *Q. J. R. Meteor. Soc.* **146,** 1999-2049 (2020).
42. Good, S. A., M. J. Martin & N. A. Rayner. EN4: quality controlled ocean temperature and salinity profiles and monthly objective analyses with uncertainty estimates. *J. Geophys. Res. Oceans* **118,** 6704-6716 (2013).

43. Gouretski, V. & Cheng, L. Correction for systematic errors in the global dataset of temperature profiles from mechanical bathythermographs. *J. Atmos. Oceanic Technol*. **37,** 841-855 (2020).
44. Behringer, D.W. Ji, M. & Leetmaa, A. An improved coupled model for ENSO prediction and implications for ocean initialization. Part I: The ocean data assimilation system. *Mon. Weather Rev.* **126,** 1013-1021 (1998).

Data availability

ERA5 SST: https://cds.climate.copernicus.eu/cdsapp#!/dataset/reanalysis-era5-single-levels-monthly-means?tab=form;

EN4.2.1: https://www.metoffice.gov.uk/hadobs/en4/download-en4-2-1.html;

EN4.2.2: https://www.metoffice.gov.uk/hadobs/en4/download-en4-2-2.html;

GODAS: https://www.psl.noaa.gov/data/gridded/data.godas.html;

CMIP6: https://esgf-node.llnl.gov/search/cmip6/.

Acknowledgements

This work was supported by the National Natural Science Foundation of China (42088101). T. T. (3rd author) was supported by the Japan Society for Promotion of Science through Grant-in-Aid for Scientific Research (B) (JSPS KAKENHI Grant number JP22H01293). T. T. (1st author) gratefully acknowledge financial support from China Scholarship Council. The numerical calculations in this paper have been done on the supercomputing system in the Supercomputing Center of Nanjing University of Information Science and Technology.

Author contributions

T.T. (1st author) and L.Q conceived the central idea of the study. T.T. (1st author) performed all analyses, prepared the figures, and wrote the paper. All authors contributed to interpreting results, discussion of associated dynamics, and writing.

Competing financial interests

The authors declare no competing financial interests.

Methods

Models and datasets.

The monthly SST (tos), precipitation (pr), multiple-level zonal (ua) and meridional wind (va), and ocean water potential temperature (thetao) in the 22 CMIP6 models (see Fig. 2) are used here. In this research, seasonal-mean during boreal summer (i.e., July-October) are analyzed. A 40-year period from 1981 to 2020 is used for the historical simulation. Since the historical runs mostly end in 2014, outputs from 2015 to 2020 are from the Shared Socioeconomic Pathway (SSP) 245 scenario. On the other hand, outputs from the last 40-year (2059-2098) of the SSP 245 scenario are used for the future projections. The MME mean is defined as the equal weight average of the 22 models. Only one ensemble (i.e., r1i1p1f1) of each CMIP6 model is used in this research.

The observational SST and precipitation in the ERA5 datasets[41] are used. The subsurface temperature for ocean includes the EN4.2.1[42], EN4.2.2[43] from the Hadley Centre and the ocean data assimilation product (i.e., GODAS)[44] from the National Centers for Environmental Prediction (NCEP). The mean of three ocean water potential temperature datasets is used in the emergent constraint method to yield the optimal constraint. The same 40-year period from 1981 to 2020 are used as the model baselines. All model outputs and reanalysis datasets are interpolated to the common 1°x1° grid.

Definitions of SST, precipitation, relative vorticity, horizonal wind speed at 850hPa and the NWPMT change in the future projections.

The change of each variable mentioned above is computed by taking the difference between the future projections (2059-2098) and historical simulations (1981-2020). Additionally, the change of each variable is normalized by the globally averaged SST change in each model to account for the different sensitivity of each model to global warming.

Inter-model EOF analysis.

The leading modes of the inter-model SST change over the equatorial Pacific (10°S-10°N, 120°E-60°W) are obtained by the conventional EOF method, applied to model-spatial dimensions:

$$\Delta SST'(m,s) \cong \sum_{i=1}^{n} \left(PC_{i,m} \times EOF_{i,s}\right).$$

Here, ΔSST denotes SST change, m denotes the model number, s represents the spatial grid, and n denotes the mode number. Prime means the deviation from the multi-model mean.

Emergent constraint method.

The emergent constraint method has been widely used to reduce uncertainty in future projections[32,33,38]. By establishing a physical linkage between the target future projection Y and the historical simulation X, the observational constraint method can be described as follows:

$$Y = aX + b.$$

Here, a is the regression coefficient, and b is the intercept. In this study, Y is the PC1 of the equatorial Pacific SST change among the CMIP6 models, or the NWPMT index change, and X is the thermocline sharpness in the historical simulations.

According to this relationship between the historical simulations and the future projections, we can obtain optimal constraint results of the PC1 and the NWPMT index change in the future.

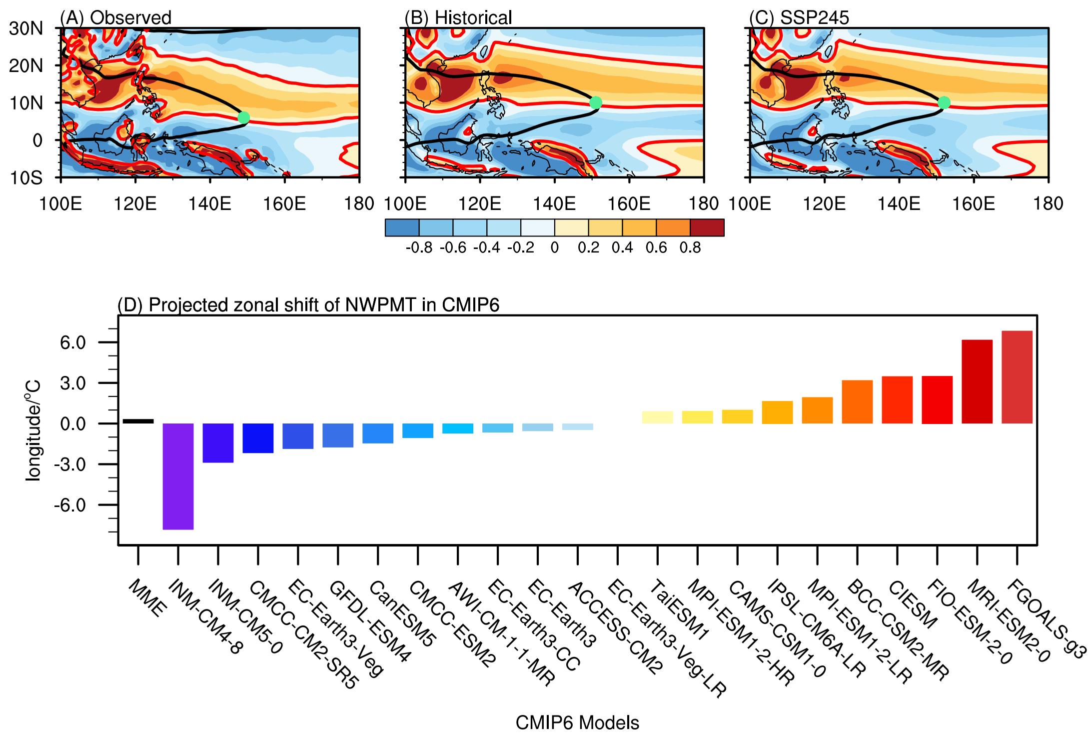

Figure 1. Geographical location of the northwestern Pacific monsoon trough (NWPMT) and its projected shift in the Coupled Model Intercomparison Project Phase 6 (CMIP6) future projections. (A), (B), (C) Climatological locations of the NWPMT (green dot) in the observed datasets (1981-2020), and the multi-model mean of the historical simulations (1981-2020) and future projections (2059-2098) in boreal summer, respectively. The color shading denotes the relative vorticity (10^{-5} s^{-1}). The black and red solid curves denote the zero-zonal wind contour (m s^{-1}) and the zero relative vorticity contour, respectively. (D) Rank of the NWPMT index change (longitude $°C^{-1}$) in the CMIP6 future projections. The black bar represents the multi-model mean. Note that the zonal shift of NWPMT has been normalized by the corresponding globally averaged SST change in each model to account for different sensitivity of each model to global warming.

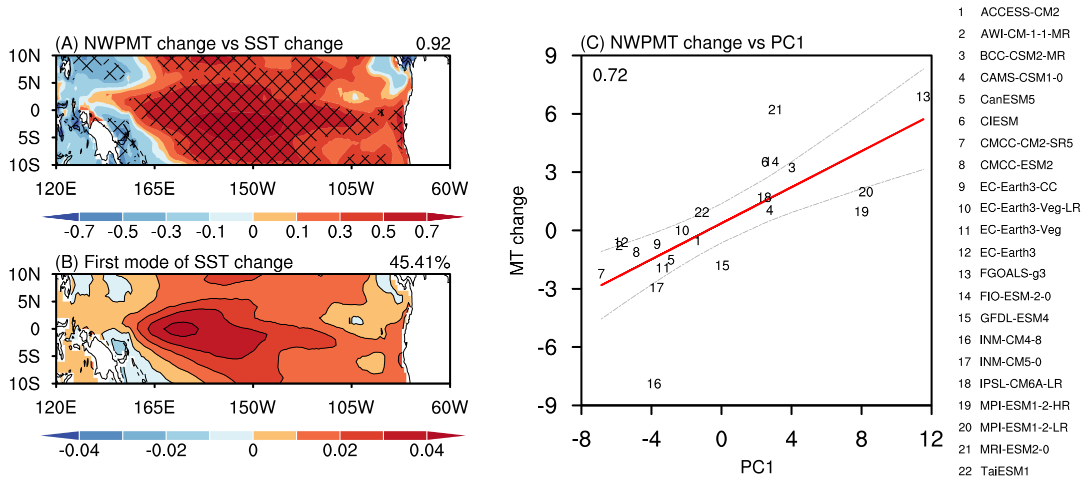

Figure 2. Correlation between the projected NWPMT and the central equatorial Pacific sea surface temperature (SST) change. (A) Inter-model correlation coefficents between the NWPMT change and the tropical Pacific SST change in CMIP6. Hatching indicates correlation coefficients significant at the 95% confidence level with a Student t-test. (B) The first emperical orthogonal function (EOF) mode of equatorial Pacific SST change among CMIP6 models. The spatial pattern correlation between panel (A) and panel (B) is indicated in the upper right of panel (A), and the variance contribution of the leading mode is indicated in the upper right of panel (B). (C) Scattor plot constructed by the principal component of the leading mode (PC1, X axis), and NWPMT change (Y axis) in each CMIP6 model. The red solid line denotes the regression line, while the gray dashed lines represent the 95% confidence range of the linear regression. Their correlation coefficient is indicated in the upper left.

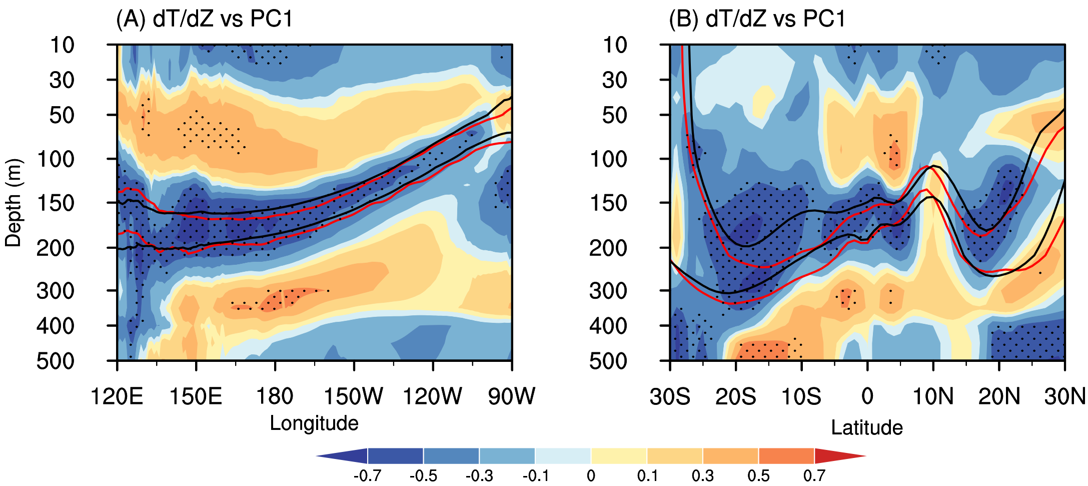

Figure 3. Correlation coefficients between PC1 and vertical ocean temperature gradient. (A) Zonal cross section of correlation coefficients averaged along the equatorial (5°S-5°N) Pacific. (B) As in (A), but for the meridional cross section averaged over 150°E-150°W. Stippling indicates correlation coefficients significant at the 95% confidence level with a Student t-test. The red and black solid curves denote the 20°C and 16°C isotherms in the mean of the observed datasets and the multi-model mean of historical simulations in the CMIP6, respectively.

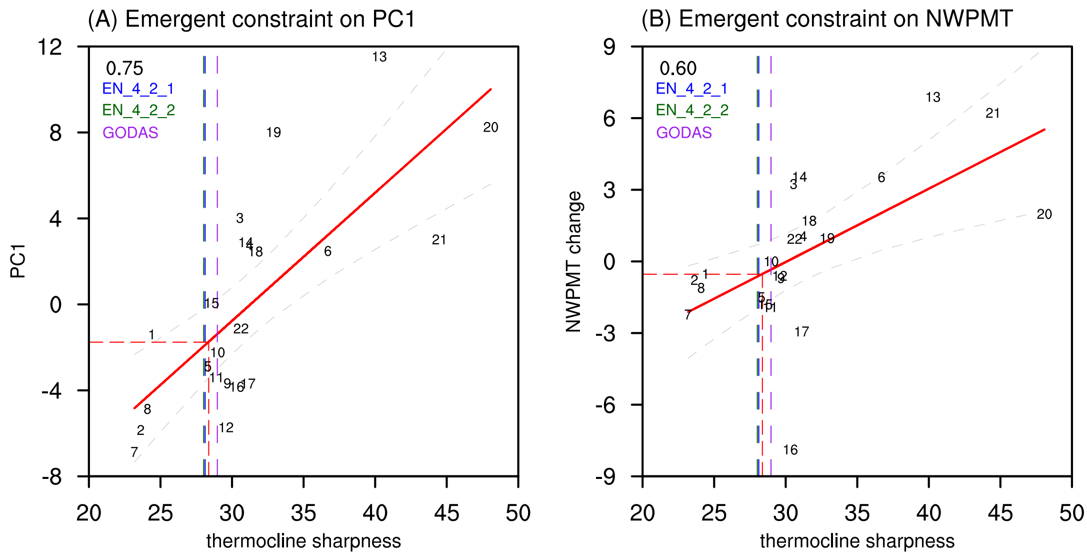

Figure 4. Inter-model relationship between simulated thermocline sharpness and future projections. (A) Inter-model correlation between thermocline sharpness (m) that is measured by the difference between the depth of 20°C and 16°C isotherms over the central equatorial Pacific (5°S-5°N, 150°E-150°W) and PC1. The red solid line denotes the linear regression line, while the gray dashed lines represent the 95% confidence range of the linear regression. The blue, green and purple vertical dashed lines denote the thermocline sharpness in the EN4.2.1, EN4.2.2 and GODAS, respecitively. The red dashed vertical line denotes the mean of three observed datasets, and the induced optimal projection according to emergent constraint is represented by the red horizonal dashed line. (B) As in (A), but for thermocline sharpness and the projected NWPMT shift. The inter-model correlation coefficent is indicated in the upper left of each panel.

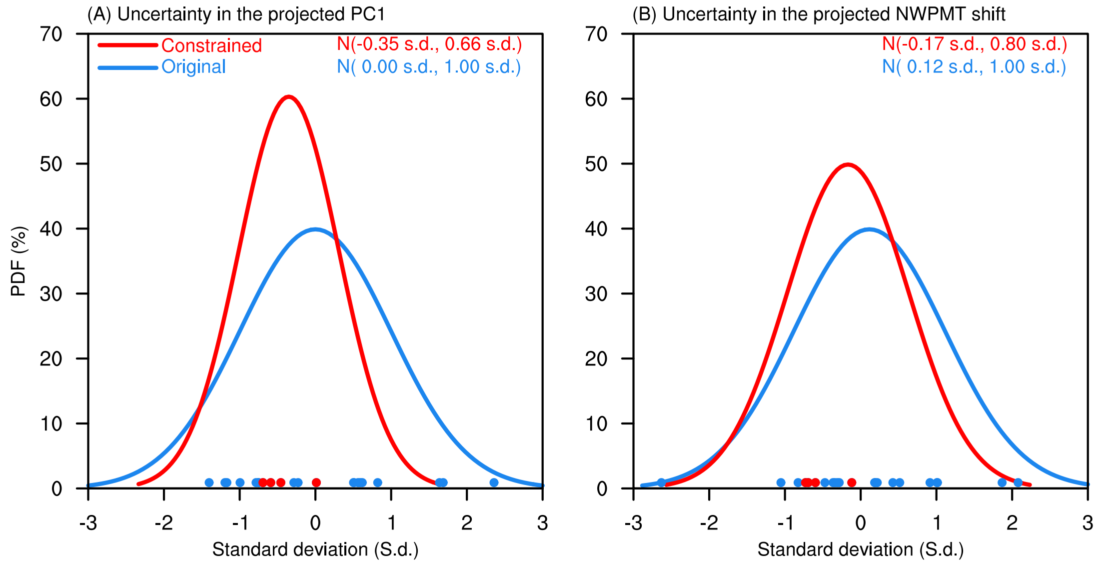

Figure 5. Probability density function of original and constrained future projections. (A) Probability density function (PDF) of the standardized principal components (PC1) of the leading mode of the equatorial Pacific SST change differences among CMIP6 models are generated under Gaussian assumption. The red (blue) curve denotes the PDF distribution of the original (constrained) PC1. The values in parentheses at the top are mean and standard deviation of the Gaussian distribution. The red and blue dots at the bottom represent four CMIP6 models with realistic thermocline sharpness and other CMIP6 models, respectively. (B) As in (A), but for the PDF distributions of the standardized NWPMT index change in CMIP6 models.

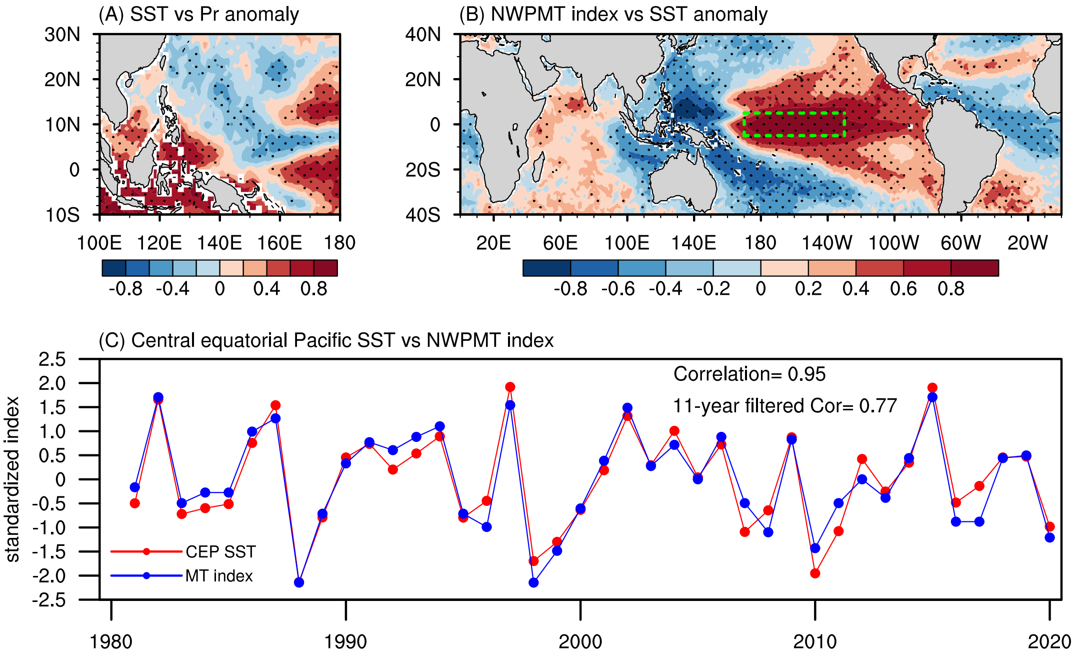

Supplementary Figure 1. Relationship between NWPMT shift and central equatorial Pacific SST variabilities in the observational datasets. (A) Point-wise linear correlation coefficients between precipitation and SST anomalies in boreal summer (July-October). (B) Linear correlation coefficients between annual NWPMT index and SST anomalies averaged over boreal summer. Stippling indicates the correlation coefficients significant at the 95% confidence level with a Student t-test. (C) Annual timeseries of the standardized NWPMT index (blue) and SST anomalies averaged over the central equatorial Pacific (5°S-5°N, 170°E-130°W, green dashed box in panel (B), red). Correlation coefficients are indicated in the upper right.

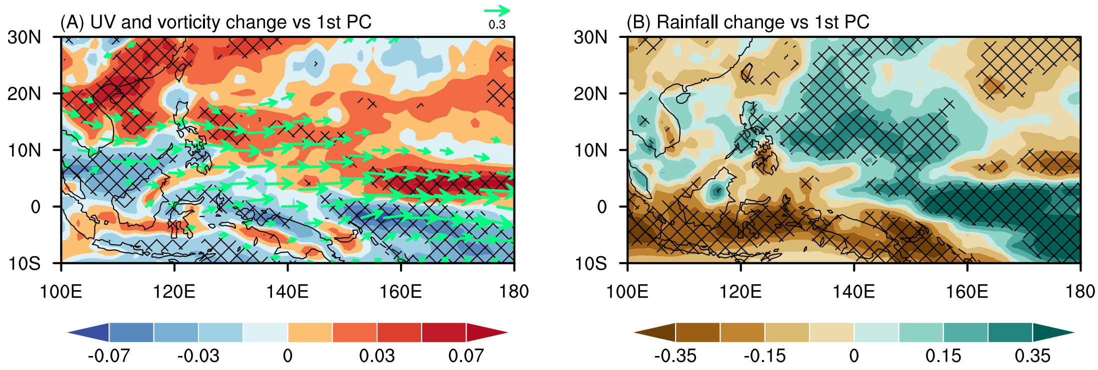

Supplementary Figure 2. Projected change of atmospheric circulations over the northwestern Pacific due to per inter-model standard deviation of the PC1. (A) Relative vorticity (10^{-5} s^{-1} °C^{-1}) and horizontal wind changes (m s^{-1} °C^{-1}) at 850 hPa due to per inter-model standard deviation of the PC1. Hatching (green vector) indicates the regression coefficients between the PC1 and relative vorticity (horizontal wind) change significant at the 95% confidence level with a Student t-test. (B) As in (A), but for the precipitation change (mm day^{-1} °C^{-1}).

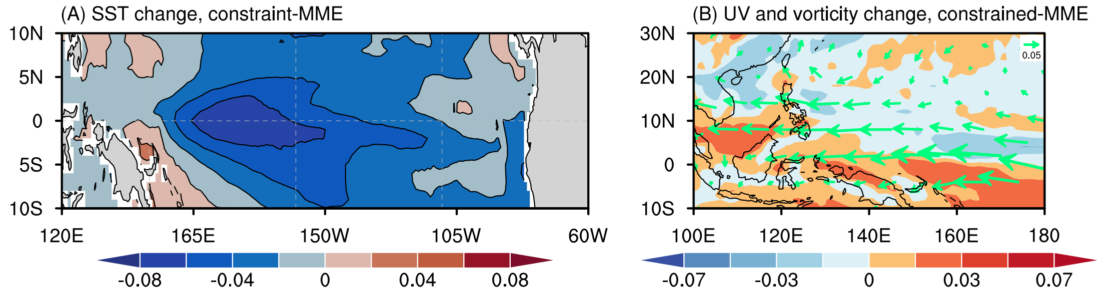

Supplementary Figure 3. Difference of projected SST, 850 hPa horizontal wind and relative vorcitity change between the constrained projections and the multi-model ensemble mean (MME). (A) Difference of SST change ($°C\ °C^{-1}$) between the projections after constraining and CMIP6 MME. (B) Differences of horizontal wind change ($m\ s^{-1}\ °C^{-1}$, green vector) and relative vorticity change ($10^{-5}\ s^{-1}\ °C^{-1}$, color shading) due to the differences of SST change.